

## FTIR Spectra and Normal-Mode Analysis of a Tetranuclear Manganese Adamantane-like Complex in Two Electrochemically Prepared Oxidation States: Relevance to the Oxygen-Evolving Complex of Photosystem II

Hendrik Visser,<sup>†,‡</sup> Christopher E. Dubé,<sup>§,¶</sup> William H. Armstrong,<sup>\*,§</sup>  
Kenneth Sauer,<sup>\*,†,‡</sup> and Vittal K. Yachandra<sup>\*,†</sup>

Contribution from the Melvin Calvin Laboratory, Physical Biosciences Division,  
Lawrence Berkeley National Laboratory, Berkeley, California 94720, Department of Chemistry,  
University of California, Berkeley, California 94720-5230, and Department of Chemistry,  
Eugene F. Merkert Chemistry Center, Boston College,  
Chestnut Hill, Massachusetts 02167-3860

Received March 20, 2002

**Abstract:** The IR spectra and normal-mode analysis of the adamantane-like compound  $[\text{Mn}_4\text{O}_6(\text{bpea})_4]^{n+}$  (bpea = *N,N*-bis(2-pyridylmethyl)ethylamine) in two oxidation states,  $\text{Mn}^{\text{IV}}_4$  and  $\text{Mn}^{\text{III}}\text{Mn}^{\text{IV}}_3$ , that are relevant to the oxygen-evolving complex of photosystem II are presented. Mn–O vibrational modes are identified with isotopic exchange,  $^{16}\text{O} \rightarrow ^{18}\text{O}$ , of the mono- $\mu$ -oxo bridging atoms in the complex. IR spectra of the  $\text{Mn}^{\text{III}}\text{Mn}^{\text{IV}}_3$  species are obtained by electrochemical reduction of the  $\text{Mn}^{\text{IV}}_4$  species using a spectroelectrochemical cell, based on attenuated total reflection [Visser, H.; et al. *Anal. Chem.* **2001**, *73*, 4374–4378]. A novel method of subtraction is used to reduce background contributions from solvent and ligand modes, and the difference and double-difference spectra are used in identifying Mn–O bridging modes that are sensitive to oxidation state change. Two strong IR bands are observed for the  $\text{Mn}^{\text{IV}}_4$  species at 745 and 707  $\text{cm}^{-1}$ , and a weaker band is observed at 510  $\text{cm}^{-1}$ . Upon reduction, the  $\text{Mn}^{\text{III}}\text{Mn}^{\text{IV}}_3$  species exhibits two strong IR bands at 745 and 680  $\text{cm}^{-1}$ , and several weaker bands are observed in the 510–425  $\text{cm}^{-1}$  range. A normal-mode analysis is performed to assign all the relevant bridging modes in the oxidized  $\text{Mn}^{\text{IV}}_4$  and reduced  $\text{Mn}^{\text{III}}\text{Mn}^{\text{IV}}_3$  species. The calculated force constants for the  $\text{Mn}^{\text{IV}}_4$  species are  $f_{\text{r}}^{\text{IV}} = 3.15$  mdyn/Å,  $f_{\text{rOr}} = 0.55$  mdyn/Å, and  $f_{\text{rMnr}} = 0.20$  mdyn/Å. The force constants for the  $\text{Mn}^{\text{III}}\text{Mn}^{\text{IV}}_3$  species are  $f_{\text{r}}^{\text{IV}} = 3.10$  mdyn/Å,  $f_{\text{rIII}} = 2.45$  mdyn/Å,  $f_{\text{rOr}} = 0.40$  mdyn/Å, and  $f_{\text{rMnr}} = 0.15$  mdyn/Å. This study provides insights for the identification of Mn–O modes in the IR spectra of the photosynthetic oxygen-evolving complex during its catalytic cycle.

### Introduction

The world's supply of oxygen is a byproduct of the water oxidation process carried out by oxygenic photosynthesis in organisms such as cyanobacteria and green plants. Water oxidation takes place in a transmembrane protein cluster, photosystem II (PS II), where it is catalyzed by the oxygen-evolving complex (OEC). A photon-induced electron abstraction from the OEC occurs during each of the four state transitions of the catalytic cycle ( $\text{S}_0 \rightarrow \text{S}_1$ ,  $\text{S}_1 \rightarrow \text{S}_2$ ,  $\text{S}_2 \rightarrow \text{S}_3$ ,  $\text{S}_3 \rightarrow [\text{S}_4] \rightarrow \text{S}_0$ ).<sup>1</sup> Dioxygen is released when the  $\text{S}_3$  state returns to the  $\text{S}_0$  state via the hypothesized  $\text{S}_4$  state.

Although progress has been made in obtaining a crystal structure of PS II,<sup>2</sup> most of our electronic and structural knowledge about the OEC has been obtained from X-ray absorption<sup>3–5</sup> and EPR spectroscopy.<sup>6–9</sup> From these studies, it is known that the OEC contains four manganese atoms which are arranged in two or three di- $\mu$ -oxo moieties and one mono- $\mu$ -oxo moiety. In addition, cofactors  $\text{Ca}^{2+}$  and  $\text{Cl}^-$  are required for water oxidation.<sup>10</sup> One or two histidines are directly ligated to one of the manganese atoms of the OEC,<sup>9</sup> and water has

\* To whom correspondence should be addressed. E-mail: Armstrong@bc.edu, KHSauer@lbl.gov, VKYachandra@lbl.gov.

<sup>†</sup> Lawrence Berkeley National Laboratory.

<sup>‡</sup> University of California, Berkeley.

<sup>§</sup> Boston College.

<sup>¶</sup> Present address: Charles Stark Draper Laboratory, 555 Technology Square, MS 37, Cambridge, MA 02139.

(1) Kok, B.; Forbush, B.; McGloin, M. *Photochem. Photobiol.* **1970**, *11*, 457–475.

(2) Zouni, A.; Witt, H. T.; Kern, J.; Fromme, P.; Krauss, N.; Saenger, W.; Orth, P. *Nature* **2001**, *409*, 739–743.

(3) Penner-Hahn, J. E. *Struct. Bonding (Berlin)* **1998**, *90*, 1–36.

(4) Robblee, J. H.; Cinco, R. M.; Yachandra, V. K. *Biochim. Biophys. Acta* **2001**, *1503*, 7–23.

(5) Yachandra, V. K.; Sauer, K.; Klein, M. P. *Chem. Rev.* **1996**, *96*, 2927–2950.

(6) Dismukes, G. C.; Siderer, Y. *Proc. Natl. Acad. Sci. U.S.A.* **1981**, *78*, 274–278.

(7) Messinger, J.; Robblee, J. H.; Yu, W. O.; Sauer, K.; Yachandra, V. K.; Klein, M. P. *J. Am. Chem. Soc.* **1997**, *119*, 11349–11350.

(8) Miller, A. F.; Brudvig, G. W. *Biochim. Biophys. Acta* **1991**, *1056*, 1–18.

(9) Peloquin, J. M.; Britt, R. D. *Biochim. Biophys. Acta* **2001**, *1503*, 96–111.

(10) Debus, R. J. *Biochim. Biophys. Acta* **1992**, *1102*, 269–352.

also been implicated as a ligand of Mn.<sup>11–14</sup> Glutamate and aspartate are thought to provide most of the other ligands.<sup>10,15</sup> During each of the first two state transitions ( $S_0 \rightarrow S_1$ ,  $S_1 \rightarrow S_2$ ) an electron is abstracted from Mn.<sup>16–19</sup> However, during the third state transition ( $S_2 \rightarrow S_3$ ) X-ray spectroscopy studies indicate that oxidation of manganese is unlikely; an electron may instead be extracted from a ligand or a nearby residue.<sup>16,17</sup> The synthesis and study of a wide variety of manganese compounds have been critical for the interpretation of the X-ray and EPR spectra of the OEC.<sup>20–29</sup>

Several mechanisms of water oxidation have been proposed. These mechanisms are divided here into four groups, in which the character of the oxygen atoms that ultimately form dioxygen is different. In these four groups the oxygen atoms come from two terminal oxygens bound to two separate manganese atoms,<sup>4,12,16,28,30–35</sup> one terminal oxygen and one oxygen not bound to the manganese cluster,<sup>4,16,28,35–39</sup> one terminal and one bridging oxygen,<sup>28,35,40</sup> or two  $\mu$ -oxo bridges.<sup>4,16,35,41,42</sup> Each of these mechanisms involves distinctly different Mn–O bonds

formed and broken during the catalytic cycle.<sup>21</sup> Therefore, it is useful to apply a technique, such as vibrational spectroscopy, that distinguishes among the different kinds of Mn–O bonds and other relevant bonds of the OEC.

Recently, vibrational spectroscopy has been added as an investigative tool to study the structure and mechanism of the OEC. Changes during the catalytic cycle in the 1800–1200  $\text{cm}^{-1}$  range, which arise from vibrations of the protein residues ligated to the OEC,<sup>14,43–49</sup> are complemented by those of the Mn–ligand vibrations, specifically the Mn–O vibrations, which occur in the 200–1000  $\text{cm}^{-1}$  range.<sup>49–52</sup> Vibrations of a water molecule in the OEC have been detected in the 2500–3700  $\text{cm}^{-1}$  range using H/D exchange studies.<sup>14,53</sup> The low frequency range is especially helpful in determining the mechanism of water oxidation. Chu et al.<sup>43,49,51</sup> were able to obtain IR difference spectra of the  $S_1 \rightarrow S_2$  transition of the OEC in the 350–1000  $\text{cm}^{-1}$  range. They identified a Mn–O–Mn vibration at 625  $\text{cm}^{-1}$  in the  $S_1$  state, which shifts to 606  $\text{cm}^{-1}$  in the  $S_2$  state (596  $\text{cm}^{-1}$  in the  $^{18}\text{O}$ -treated sample). Low-frequency (220–620  $\text{cm}^{-1}$ ) resonance Raman spectra of the OEC were obtained by Cua et al.<sup>54</sup> They observed two scattering peaks at 348 and 476  $\text{cm}^{-1}$  which are sensitive to isotopic exchange of D for H and were tentatively assigned to either a Mn–OH or Mn–OH<sub>2</sub> vibration. Such vibrational assignments of the OEC are based on studies of known manganese compounds.<sup>49,55–61</sup>

Vibrational spectra of manganese model compounds are indispensable for the interpretation of the IR and Raman spectra of the OEC. There are several multinuclear Mn complexes that have been prepared to understand the spectral properties of the Mn complex in the OEC. An excellent summary of the low-frequency vibrational modes observed in such complexes is presented in a review by Babcock and co-workers<sup>49</sup> (see also Results and Discussion). However, only a few manganese model compounds have been extensively studied by IR or Raman spectroscopy using isotopic exchange, such as  $^{16}\text{O} \rightarrow ^{18}\text{O}$ ,<sup>23,56</sup> and normal-mode analysis.<sup>62</sup> Isotopic exchange is necessary to distinguish Mn–O vibrational modes from modes which involve

- (11) Hillier, W.; Messinger, J.; Wydrzynski, T. *Biochemistry* **1998**, *37*, 16908–16914.
- (12) Hillier, W.; Wydrzynski, T. *Biochim. Biophys. Acta* **2001**, *1503*, 197–209.
- (13) Messinger, J.; Badger, M.; Wydrzynski, T. *Proc. Natl. Acad. Sci. U.S.A.* **1995**, *92*, 3209–3213.
- (14) Noguchi, T.; Sugiura, M. *Biochemistry* **2000**, *39*, 10943–10949.
- (15) Debus, R. J. In *Manganese and Its Role in Biological Processes*; Sigel, A., Sigel, H., Eds.; Marcel Dekker: New York, 2000; Vol. 37, pp 657–711.
- (16) Messinger, J.; Robblee, J. H.; Bergmann, U.; Fernandez, C.; Glatzel, P.; Visser, H.; Cinco, R. M.; McFarlane, K. L.; Bellacchio, E.; Pizarro, S. A.; Cramer, S. P.; Sauer, K.; Klein, M. P.; Yachandra, V. K. *J. Am. Chem. Soc.* **2001**, *123*, 7804–7820.
- (17) Roelofs, T. A.; Liang, M. C.; Latimer, M. J.; Cinco, R. M.; Rompel, A.; Andrews, J. C.; Sauer, K.; Yachandra, V. K.; Klein, M. P. *Proc. Natl. Acad. Sci. U.S.A.* **1996**, *93*, 3335–3340.
- (18) Ono, T.; Noguchi, T.; Inoue, Y.; Kusunoki, M.; Matsushita, T.; Oyanagi, H. *Science* **1992**, *258*, 1335–1337.
- (19) Iuzzolino, L.; Dittmer, J.; Dörner, W.; Meyer-Klaucke, W.; Dau, H. *Biochemistry* **1998**, *37*, 17112–17119.
- (20) Christou, G. *Acc. Chem. Res.* **1989**, *22*, 328–335.
- (21) Armstrong, W. H. In *Manganese Redox Enzymes*; Pecoraro, V. L., Ed.; VCH Publishers: New York, 1992; pp 261–286.
- (22) Cinco, R. M.; Rompel, A.; Visser, H.; Aromí, G.; Christou, G.; Sauer, K.; Klein, M. P.; Yachandra, V. K. *Inorg. Chem.* **1999**, *38*, 5988–5998.
- (23) Cooper, S. R.; Calvin, M. J. *J. Am. Chem. Soc.* **1977**, *99*, 6623–6630.
- (24) Pecoraro, V. L.; Baldwin, M. J.; Gelasco, A. *Chem. Rev.* **1994**, *94*, 807–826.
- (25) Pecoraro, V. L.; Hsieh, W.-Y. In *Manganese and Its Role in Biological Processes*; Sigel, A., Sigel, H., Eds.; Marcel Dekker Inc.: New York, 2000; Vol. 37, pp 429–504.
- (26) Visser, H.; Anxolabehère-Mallart, E.; Bergman, U.; Glatzel, P.; Robblee, J. H.; Cramer, S. P.; Girerd, J.-J.; Sauer, K.; Klein, M. P.; Yachandra, V. K. *J. Am. Chem. Soc.* **2001**, *123*, 7031–7039.
- (27) Wiegardt, K. *Angew. Chem., Int. Ed. Engl.* **1989**, *28*, 1153–1172.
- (28) Limburg, J.; Brudvig, G. W.; Crabtree, R. H. In *Biomimetic oxidations catalyzed by transition metal complexes*; Meunier, B., Ed.; Imperial College Press: London, 2000; pp 509–541.
- (29) Ruettinger, W. F.; Campana, C.; Dismukes, G. C. *J. Am. Chem. Soc.* **1997**, *119*, 6670–6671.
- (30) Haumann, M.; Junge, W. *Biochim. Biophys. Acta* **1999**, *1411*, 86–91.
- (31) Hoganson, C. W.; Babcock, G. T. In *Manganese and Its Role in Biological Processes*; Sigel, A., Sigel, H., Eds.; Marcel Dekker Inc.: New York, 2000; Vol. 37, pp 613–656.
- (32) Messinger, J. *Biochim. Biophys. Acta* **2000**, *1459*, 481–488.
- (33) Renger, G. *Biochim. Biophys. Acta* **2001**, *1503*, 210–228.
- (34) Tommos, C.; Babcock, G. T. *Acc. Chem. Res.* **1998**, *31*, 18–25.
- (35) Kambara, T.; Govindjee. *Proc. Natl. Acad. Sci. U.S.A.* **1985**, *82*, 6119–6123.
- (36) Dau, H.; Iuzzolino, L.; Dittmer, J. *Biochim. Biophys. Acta* **2001**, *1503*, 24–39.
- (37) Kuzek, D.; Pace, R. J. *Biochim. Biophys. Acta* **2001**, *1503*, 123–137.
- (38) Siegbahn, P. E. M.; Crabtree, R. H. *J. Am. Chem. Soc.* **1999**, *121*, 117–127.
- (39) Vrettos, J. S.; Limburg, J.; Brudvig, G. W. *Biochim. Biophys. Acta* **2001**, *1503*, 229–245.
- (40) Nugent, J. H. A.; Rich, A. M.; Evans, M. C. W. *Biochim. Biophys. Acta* **2001**, *1503*, 138–146.
- (41) Brudvig, G. W.; Beck, W. F.; De Paula, J. C. *Annu. Rev. Biophys. Biophys. Chem.* **1989**, *18*, 25–46.
- (42) Christou, G.; Vincent, J. B. *Biochim. Biophys. Acta* **1987**, *895*, 259–274.
- (43) Chu, H.-A.; Hillier, W.; Law, N. A.; Sackett, H.; Haymond, S.; Babcock, G. T. *Biochim. Biophys. Acta* **2000**, *1459*, 528–532.
- (44) Noguchi, T.; Inoue, Y.; Tang, X. S. *Biochemistry* **1999**, *38*, 10187–10195.
- (45) Noguchi, T.; Ono, T. A.; Inoue, Y. *Biochim. Biophys. Acta* **1993**, *1143*, 333–336.
- (46) Noguchi, T.; Ono, T. A.; Inoue, Y. *Biochim. Biophys. Acta* **1995**, *1232*, 59–66.
- (47) Steenhuis, J. J.; Barry, B. A. *J. Phys. Chem. B* **1997**, *101*, 6652–6660.
- (48) Steenhuis, J. J.; Hutchison, R. S.; Barry, B. A. *J. Biol. Chem.* **1999**, *274*, 14609–14616.
- (49) Chu, H. A.; Hillier, W.; Law, N. A.; Babcock, G. T. *Biochim. Biophys. Acta* **2001**, *1503*, 69–82.
- (50) Chu, H.-A.; Debus, R. J.; Babcock, G. T. *Biochemistry* **2001**, *40*, 2312–2316.
- (51) Chu, H.-A.; Gardner, M. T.; O'Brien, J. P.; Babcock, G. T. *Biochemistry* **1999**, *38*, 4533–4541.
- (52) Chu, H.-A.; Sackett, H.; Babcock, G. T. *Biochemistry* **2000**, *39*, 14371–14376.
- (53) Fischer, G.; Wydrzynski, T. *J. Phys. Chem. B* **2001**, *105*, 12894–12901.
- (54) Cua, A.; Stewart, D. H.; Reifler, M. J.; Brudvig, G. W.; Bocian, D. F. *J. Am. Chem. Soc.* **2000**, *122*, 2069–2077.
- (55) Cooper, S. R.; Dismukes, G. C.; Klein, M. P.; Calvin, M. J. *J. Am. Chem. Soc.* **1978**, *100*, 7248–7252.
- (56) Dave, B. C.; Czernuszewicz, R. S. *Inorg. Chim. Acta* **1994**, *227*, 33–41.
- (57) Dave, B. C.; Czernuszewicz, R. S. *Inorg. Chim. Acta* **1998**, *281*, 25–35.
- (58) Davidson, G. *Spectroscopic Properties of Inorganic and Organometallic Compounds*; The Royal Society of Chemistry, U.K.: London, 1997; Vol. 30.
- (59) Nakamoto, K. *Infrared and Raman Spectra of Inorganic and Coordination Compounds*, 5th ed.; John Wiley & Sons: New York, 1997.
- (60) Ross, S. D. *Inorganic Infrared and Raman Spectra*; McGraw-Hill: London, 1972.
- (61) Baldwin, M. J.; Stemmler, T. L.; Riggs-Gelasco, P. J.; Kirk, M. L.; Penner-Hahn, J. E.; Pecoraro, V. L. *J. Am. Chem. Soc.* **1994**, *116*, 11349–11356.

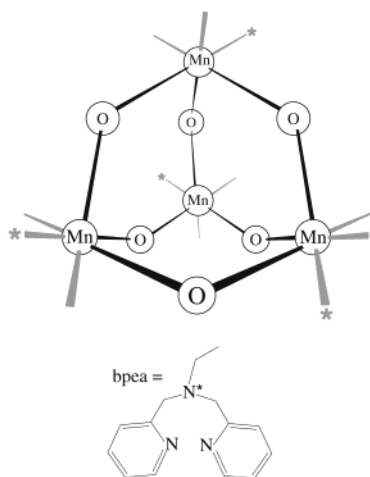


**Figure 1.** Adamantane-like manganese compound  $[\text{Mn}^{\text{IV}}_4\text{O}_6(\text{bpea})_4]^{4+}$ , with the nonaromatic nitrogen of each bpea ligand indicated by an asterisk.

other parts of the complex. Normal-mode analysis of the complexes is required to understand the pattern of the identified vibrations and to extract force constants. These force constants can be used to predict and analyze the vibrational spectra of other compounds and the OEC. The compounds for which the Mn–ligand force constants are known are various manganese oxide compounds ( $\text{MnO}_3\text{X}^{n-}$ , with  $\text{X} = \text{O}, \text{F}, \text{or Cl}$ ),<sup>63–65</sup> manganese halide compounds ( $\text{Mn}^{\text{II}}\text{X}_4^{2-}$ , with  $\text{X} = \text{Cl}, \text{Br}, \text{or I}$ ),<sup>66,67</sup> compounds that contain a Mn–oxygen ligand unit held by porphyrin derivatives,<sup>68</sup> and a mono- $\mu$ -oxo compound.<sup>62</sup> Only the last compound contains a moiety which is structurally relevant to the OEC. Therefore, more vibrational studies are needed of manganese compounds in different oxidation states relevant to the catalytic cycle of the OEC. It is not always possible to obtain solid homologous multinuclear Mn compounds in different oxidation states, but it is often possible to generate such redox states electrochemically in solution. Therefore, a technique which combines electrochemistry and IR spectroscopy has been utilized to advantage, as described below.

In this paper we present the IR spectra and a normal-mode analysis of the tetranuclear adamantane-like Mn compounds  $[\text{Mn}^{\text{IV}}_4\text{O}_6(\text{bpea})_4]^{4+}$  (**1**) and  $[\text{Mn}^{\text{IV}}_3\text{Mn}^{\text{III}}\text{O}_6(\text{bpea})_4]^{3+}$  (**2**), with  $^{16}\text{O}$  and  $^{18}\text{O}$  in the bridging moiety, where bpea (*N,N*-bis(2-pyridylmethyl)ethylamine) is the terminal ligand (Figure 1).<sup>69</sup> The ligand bpea has one nonaromatic nitrogen (indicated by an asterisk in Figure 1) and two aromatic nitrogens ligated to Mn, which causes the compound to approach  $S_4$  symmetry. The IR spectrum of **1** as a solid reveals a Mn–O–Mn stretch mode at  $709\text{ cm}^{-1}$ , which shifts to  $675\text{ cm}^{-1}$  upon  $^{16}\text{O}$ -to- $^{18}\text{O}$  exchange.<sup>69</sup> This frequency is close to  $730\text{ cm}^{-1}$ , which was identified as a Mn–O vibration for the structurally analogous  $[\text{Mn}^{\text{IV}}_4\text{O}_6$ -

$(\text{tacn})_4]^{4+}$  (**3**), where tacn is 1,4,7-triazacyclononane.<sup>70</sup> In contrast to bpea, tacn has three equivalent nonaromatic nitrogens ligated to Mn, with the compound close to  $T_d$  symmetry.

The bpea compound in acetonitrile has a reversible wave in the cyclic voltammogram at  $E_{1/2} = 0.104\text{ V}$  versus SCE (standard calomel electrode) for the  $(\text{Mn}^{\text{IV}}_4 + e^- \rightleftharpoons \text{Mn}^{\text{III}}\text{Mn}^{\text{IV}}_3)$  redox couple. In the present work a novel attenuated total reflection (ATR) spectroelectrochemical cell<sup>71</sup> is used to obtain IR difference spectra of the adamantane-like compound in the two oxidation states. The reversibility of the redox couple is advantageously utilized to distinguish IR frequencies of the compound from nonreversible background signals. In addition,  $^{16}\text{O}$ – $^{18}\text{O}$  isotopic exchange is used to distinguish Mn–O bridging modes from the terminal ligand modes. This is the first time that such an IR study has been performed on a manganese compound in two oxidation states in solution relevant to the OEC, and a normal-mode analysis has been used to identify the bridging Mn–O modes sensitive to the oxidation state of Mn.

## Experimental Section

**Synthesis.** Synthesis and isotopic exchange of the bridging oxygen atoms of **1** were performed as described by Dubé et al.,<sup>69</sup> where the counterion is either  $\text{Br}^-$  (for the solid compound IR spectra) or  $\text{ClO}_4^-$  (for the acetonitrile solution IR difference spectra during electrochemistry). During the isotopic exchange a 90% replacement of  $^{16}\text{O}$  by  $^{18}\text{O}$  was achieved.<sup>69</sup>

**Electrochemistry.** A home-built spectroelectrochemical apparatus described in detail elsewhere<sup>71</sup> was used to measure the solution IR spectra of the redox species during electrochemistry. The apparatus consists of an electrochemical cell made of Teflon, which interfaces with an ASI DuraSamplIR (Applied Systems Inc., Annapolis, MD) ATR accessory.<sup>72,73</sup> The ATR device has a wide spectral range of  $16700$ – $250\text{ cm}^{-1}$ , and a small opaque region of  $2250$ – $1900\text{ cm}^{-1}$ . Pt gauze was used for both the working and counter electrodes. The counter electrode was placed inside a glass tube fitted with a fritted glass disk to minimize diffusion of electrochemical products. The nonaqueous  $[\text{CH}_3\text{CN}, 0.1\text{ M TBA}(\text{PF}_6); \text{TBA} = \text{tert-butylammonium}] \text{Ag}/\text{AgClO}_4$  (0.01 M) reference electrode (determined to be 270 mV more positive than SCE) was isolated from the bulk solution by an additional electrolyte bridge (a glass tube fitted with a Vycor tip), which was changed between samples to avoid contamination.

The electrolyte solution (0.1 M TBA( $\text{PF}_6$ ) in acetonitrile) was dried over  $\text{Al}_2\text{O}_3$  and bubbled with Ar prior to each experiment. Sample solutions (0.8 mL) of either 2.8 mM  $[\text{Mn}^{\text{IV}}_4^{16}\text{O}_6(\text{bpea})_4](\text{ClO}_4)_4$  or 2.5 mM  $[\text{Mn}^{\text{IV}}_4^{18}\text{O}_6(\text{bpea})_4](\text{ClO}_4)_4$  were kept under a constant purge of Ar during electrochemistry. Ar gas was bubbled through dry acetonitrile (dried with  $\text{Al}_2\text{O}_3$ ) to minimize evaporation and small changes in the concentration. Electrochemistry was performed using a BAS CV-27 voltammeter controller. Reduction of the  $\text{Mn}^{\text{IV}}_4$  complex was done at  $-0.7\text{ V}$  and oxidation at  $+0.3\text{ V}$  vs the  $\text{Ag}/\text{AgClO}_4$  reference electrode ( $E_{1/2} = -0.2\text{ V}$  vs  $\text{Ag}/\text{AgClO}_4$ , and  $+0.10\text{ V}$  vs SCE<sup>69</sup>).

**IR Spectroscopy.** A Bruker IFS88 Fourier transform infrared (FTIR) spectrometer was used to collect the infrared data. The spectrometer contains a KBr beam-splitter and a broad-band mercury–cadmium–telluride (MCT) detector (lower cutoff  $400\text{ cm}^{-1}$ ). KBr disks were used to obtain the IR spectra (averaged over 100 scans) of both the solid  $^{16}\text{O}$  and  $^{18}\text{O}$  adamantane-like  $[\text{Mn}^{\text{IV}}_4\text{O}_6(\text{bpea})_4]\text{Br}_4$  compounds, at a resolution of  $1\text{ cm}^{-1}$ .

(62) Sheats, J. E.; Czernuszewicz, R. S.; Dismukes, G. C.; Rheingold, A. L.; Petrouleas, V.; Stubbe, J.; Armstrong, W. H.; Beer, R. H.; Lippard, S. J. *J. Am. Chem. Soc.* **1987**, *109*, 1435–1444.

(63) Gonzalez-Vilchez, F.; Griffith, W. P. *J. Chem. Soc., Dalton Trans.* **1972**, 1416–1421.

(64) Varetto, E. L.; Filgueira, R. R.; Müller, A. *Spectrochim. Acta* **1981**, *37A*, 369–373.

(65) Varetto, E. L.; Müller, A. *Z. Anorg. Allg. Chem.* **1978**, *422*, 230–234.

(66) Edwards, H. G. M.; Ware, M. J.; Woodward, L. A. *Chem. Commun.* **1968**, 540–541.

(67) Edwards, H. G. M.; Woodward, L. A.; Gall, M. J.; Ware, M. J. *Spectrochim. Acta, Part A* **1970**, *26*, 287–290.

(68) Czernuszewicz, R. S.; Su, Y. O.; Stern, M. K.; Macor, K. A.; Kim, D.; Groves, J. T.; Spiro, T. G. *J. Am. Chem. Soc.* **1988**, *110*, 4158–4165.

(69) Dubé, C. E.; Wright, D. W.; Pal, S.; Bonitatebus, P. J.; Armstrong, W. H. *J. Am. Chem. Soc.* **1998**, *120*, 3704–3716.

(70) Wieghardt, K.; Bossek, U.; Gebert, W. *Angew. Chem., Int. Ed. Engl.* **1983**, *22*, 328–329.

(71) Visser, H.; Curtright, A. E.; McCusker, J. K.; Sauer, K. *Anal. Chem.* **2001**, *73*, 4374–4378.

(72) Milosevic, M.; Sting, D.; Rein, A. *Spectroscopy* **1995**, *10*, 44–49.

(73) Sheridan, R. E.; Rein, A. *J. R&D* **1991**, *33*, 100–102.

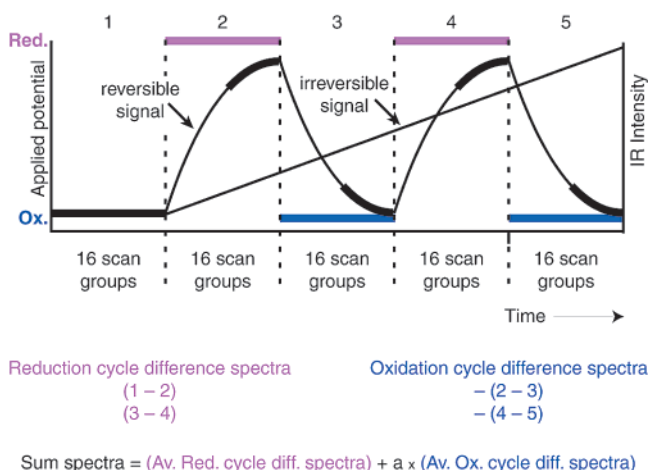


**Figure 2.** Schematic of the data collection protocol used to obtain the ( $\text{Mn}^{\text{IV}}_4 - \text{Mn}^{\text{III}}\text{Mn}^{\text{IV}}_3$ ) difference spectra. Each experiment contains two full redox cycles that consist of five redox steps. During the first redox step (labeled 1) no potential is applied; i.e., spectra are taken of the compound in the oxidized state. The first step is followed by four redox steps by alternating reducing (labeled 2 and 4) and oxidizing potentials (labeled 3 and 5) applied to the solution. This protocol enables us to obtain four spectra from two complete redox cycles. Only the maxima and minima of the oscillating IR intensity are used to calculate the difference spectra from the oxidation (2 minus 3, and 4 minus 5) and reduction cycles (1 minus 2, and 3 minus 4), indicated by the thicker lines in the schematic. The difference spectra from the oxidation cycle are multiplied by  $-1$ , so that for both redox steps the signals due to the  $\text{Mn}^{\text{IV}}_4$  species are positive and are negative for the  $\text{Mn}^{\text{III}}\text{Mn}^{\text{IV}}_3$  species. Consequently, reversible features have the same sign in the difference spectra during both the reduction and oxidation cycles, and nonreversible features have the opposite sign. Therefore, when the averaged difference spectra from the reduction and oxidation cycle are added, the nonreversible background signals are eliminated and only the reversible features remain in the Sum spectrum. The Sum spectra are calculated by adding a fraction,  $a$ , of the averaged difference spectrum during the oxidation cycle from the difference spectrum during the reduction cycle, with the objective of minimizing the irreversible signals in the Sum spectrum over the whole  $400\text{--}4000\text{ cm}^{-1}$  range.

The solution IR spectra during the electrochemistry were taken at a resolution of  $4\text{ cm}^{-1}$  and were recorded in rapid scan mode ( $128\text{ ms}$  per scan). The data collection protocol has been described previously<sup>71</sup> and is summarized here briefly (see Figure 2). The experiments were performed by alternating between reduction and oxidation conditions, enabling us to make a distinction between electrochemically reversible and nonreversible signals. Each experiment had a sequence of different redox steps: no potential applied (step 1), reduction (step 2), oxidation (step 3), reduction (step 4), oxidation (step 5). During the first redox step no potential is applied because the compound is already in the oxidized state. This sequence enables us to calculate two difference spectra during the reduction cycle of the  $\text{Mn}^{\text{IV}}_4$  species (oxidized minus reduced), and two difference spectra during the oxidation cycle of the  $\text{Mn}^{\text{III}}\text{Mn}^{\text{IV}}_3$  species (reduced minus oxidized).

During a reduction or oxidation step, 1600 scans were taken and collected into 16 separate groups (100 scans per group). Electrochemically reversible signals have successive maxima and minima in the signal intensity as a consequence of the redox sequence. Only the maxima and minima of the oscillating IR intensity are used to calculate the difference spectra, indicated by the thicker lines in Figure 2. The time profile of various IR signals during the electrochemistry was studied to determine what groups need to be discarded. The averaged maximum and minimum spectra were subtracted from each other to obtain the difference spectra during the reduction and oxidation cycles, respectively (Figure 2).

To enhance the signal-to-noise ratio of the difference spectra, this redox sequence is repeated three times for each sample,  $^{16}\text{O}$  and  $^{18}\text{O}$ . The electrochemical solution is maintained after each redox sequence

under oxidizing conditions for about 30 min to return the sample to the oxidized state. This conversion was not complete due to diffusion limitations; consequently, the IR difference signals of the second and third redox sequences were smaller than those for the first redox sequence. To correct for this difference in signal intensity, the averaged reduction and oxidation spectra were calculated by weighting the spectra of each redox sequence by the intensity of the reversible  $1030/1022\text{ cm}^{-1}$  difference signal. This corrected the differences in intensity due to the incomplete oxidation between experiments.

All of the difference spectra are presented such that features due to the oxidized species  $\text{Mn}^{\text{IV}}_4$  are positive and those for the reduced species  $\text{Mn}^{\text{III}}\text{Mn}^{\text{IV}}_3$  are negative. Therefore, reversible features have the same sign in the difference spectra during both the reduction and oxidation cycles, and nonreversible features have the opposite sign. When the averaged difference spectra from the reduction and oxidation cycles are added, the nonreversible background signals are, in principle, eliminated and only the reversible features remain in the Sum spectrum (shown in Figures 4, 5, 6, and 8).

**Normal-Mode Analysis.** Normal-mode analysis of the adamantane-like compound, which is described in detail elsewhere,<sup>74</sup> was performed using the GF-matrix method.<sup>75</sup> The linear algebra calculations of the normal-mode analysis were performed using Mathematica 3.0 (Wolfram Research). The frequencies of the normal modes were matched with the observed frequencies by varying the force constants in steps of  $0.05\text{ mdy}/\text{\AA}$ . The stretch force constants used for simulations of **1** are (1) the stretching force constant of the  $\text{Mn}^{\text{IV}}\text{--O}$  bonds,  $f_{\text{IV}}$ , and (2) the stretching coupling constants between two adjacent bonds with oxygen,  $f_{\text{O}_2}$ , or manganese,  $f_{\text{Mn}_2}$ , at the apex. In the normal-mode simulations of **2** the stretch force constant of the  $\text{Mn}^{\text{III}}\text{--O}$  bonds,  $f_{\text{III}}$ , is also included.

## Results and Discussion

### FTIR Spectra of the Solid $[\text{Mn}^{\text{IV}}_4\text{O}_6(\text{bpea})_4]^{4+}$ Compound.

Isotopic exchange of the bridging oxygen atoms is used to distinguish the predominant  $\text{Mn}\text{--O}$  vibrational modes of the adamantane-like compound from modes that do not involve oxygen atoms, such as vibrations of the terminal ligand bpea. The FTIR absorption spectra of the solid  $[\text{Mn}^{\text{IV}}_4^{16}\text{O}_6(\text{bpea})_4]^{4+}$  (black) and  $[\text{Mn}^{\text{IV}}_4^{18}\text{O}_6(\text{bpea})_4]^{4+}$  (red) compounds are shown in Figure 3. The isotope-sensitive vibrational modes are indicated by arrows. The most intense band in the spectrum of the  $^{16}\text{O}$  compound is at  $707\text{ cm}^{-1}$ , and a weaker band occurs at  $510\text{ cm}^{-1}$ . These bands shift to  $674$  and  $490\text{ cm}^{-1}$ , respectively, in the  $^{18}\text{O}$  spectrum.

Another  $\text{Mn}\text{--O}$  mode, detected as a shoulder at  $\sim 745\text{ cm}^{-1}$  in the  $^{16}\text{O}$  absorption spectra, is not present in the  $^{18}\text{O}$  spectrum. This transition is evident in the  $^{16}\text{O}\text{--}^{18}\text{O}$  difference spectrum (blue curve in Figure 3). In the difference spectrum the shoulder at  $745\text{ cm}^{-1}$  is a broad vibrational band which overlaps the  $707/674\text{ cm}^{-1}$  difference signal. It is not obvious where the  $^{18}\text{O}$  companion of this broad band appears. However, in the difference spectrum the  $707\text{ cm}^{-1}$  signal has a smaller intensity than the  $674\text{ cm}^{-1}$  signal. Upon isotopic exchange, only the frequency of vibrational modes is expected to change significantly, while the intensity of the transition only changes minimally. Therefore, this change in signal intensity is an indication that the  $^{18}\text{O}$  companion of the  $745\text{ cm}^{-1}$  peak is underneath the  $707\text{ cm}^{-1}$ . Figure 4 shows that the difference signal around  $700\text{ cm}^{-1}$  can be simulated by two  $^{16}\text{O}$  absorption

(74) Visser, H. Ph.D. thesis, University of California, Berkeley, 2001, LBNL-47934.

(75) Wilson, E. B.; Decius, J. C.; Cross, P. C. *Molecular Vibrations: The Theory of Infrared and Raman Vibrational Spectra*; Dover Publications: New York, 1955.

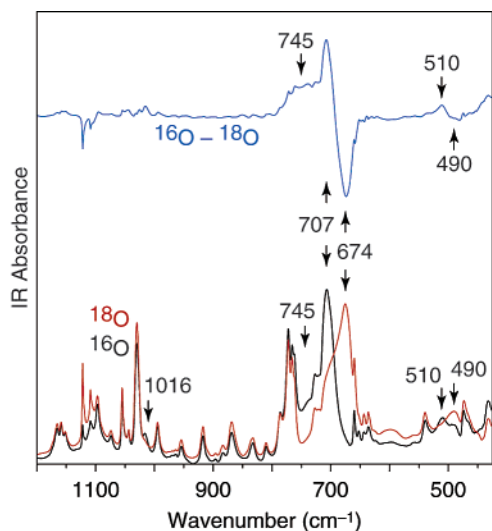


**Figure 3.** FTIR absorption spectra of the solid  $[\text{Mn}^{\text{IV}}_4^{16}\text{O}_6(\text{bpea})_4]^{4+}$  (black) and  $[\text{Mn}^{\text{IV}}_4^{18}\text{O}_6(\text{bpea})_4]^{4+}$  (red) compounds in KBr pellets, at a resolution of  $1\text{ cm}^{-1}$ , average of 100 scans. The FTIR ( $^{16}\text{O}$ – $^{18}\text{O}$ ) difference spectrum (blue) is obtained by minimizing the contribution of the bpea modes. Arrows indicate frequencies of major difference peaks between the two isotopic spectra.

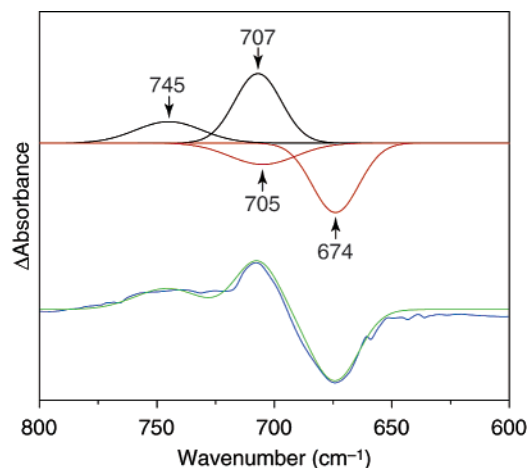


**Figure 4.** Simulation of the ( $^{16}\text{O}$ – $^{18}\text{O}$ ) FTIR difference signal around  $700\text{ cm}^{-1}$  of the  $[\text{Mn}^{\text{IV}}_4\text{O}_6(\text{bpea})_4]^{4+}$  compound (blue line), fitted with four Gaussian absorption curves (black and red lines, green is the sum of the Gaussian curves). The two positive black Gaussian curves represent the absorption bands of the  $^{16}\text{O}$  species at  $745$  and  $707\text{ cm}^{-1}$ , with bandwidths at half-height of  $20$  and  $14\text{ cm}^{-1}$ , respectively. The two negative red curves are the companion modes of the  $^{18}\text{O}$  species at  $705$  and  $674\text{ cm}^{-1}$ , with bandwidths and intensity identical to those of the  $^{16}\text{O}$  Gaussians curves.

bands at  $745$  and  $707\text{ cm}^{-1}$  (black curves), and two  $^{18}\text{O}$  absorption bands at  $705$  and  $674\text{ cm}^{-1}$  (red curves). This suggests that the  $745\text{ cm}^{-1}$  mode shifts to  $705\text{ cm}^{-1}$  upon isotopic exchange and is underneath the  $^{16}\text{O}$  species  $707\text{ cm}^{-1}$  mode in the difference spectrum.

The  $510/490\text{ cm}^{-1}$  difference signal is not strong enough to be clearly distinguished from the other signals due to the small differences in amounts of free bpea molecules, counterions, and captured solvent molecules between the  $^{16}\text{O}$  and  $^{18}\text{O}$  solid samples. Only difference signals with strong intensity can be identified when the two solid compounds are compared.

A weak absorption band which is observed at about  $1016\text{ cm}^{-1}$  for the  $^{16}\text{O}$  compound is not present in the  $^{18}\text{O}$  compound. This vibrational mode could be the first overtone of the  $510\text{ cm}^{-1}$  mode. However, the  $^{18}\text{O}$  band of this overtone mode,

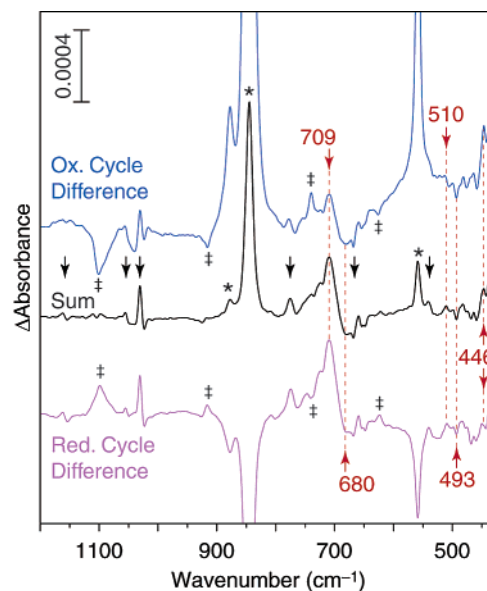


**Figure 5.** FTIR (oxidized – reduced) difference spectra of a  $2.8\text{ mM } [\text{Mn}^{\text{IV}}_4^{16}\text{O}_6(\text{bpea})_4]^{4+}/0.1\text{ M TBA}(\text{PF}_6)$  acetonitrile solution. The Sum spectrum (black) is the sum of the averaged difference spectrum from the reduction cycle (purple) and the averaged difference spectrum from the oxidation cycle (blue). The details are explained in the Experimental Section and in the caption for Figure 2. Irreversible signals due to decomposition of the electrolyte solution are indicated by ‡, and those due to changes in counterion  $\text{PF}_6^-$  concentration are indicated by \*. Reversible signals are indicated by black and red arrows; the red arrows indicate signals sensitive to the  $^{16}\text{O}$ – $^{18}\text{O}$  isotopic exchange (see Figure 6). Positive reversible signals are due to the  $\text{Mn}^{\text{IV}}_4$  oxidation state, and negative signals are due to the  $\text{Mn}^{\text{III}}\text{Mn}^{\text{IV}}_3$  oxidation state.

expected to be near  $980\text{ cm}^{-1}$ , is not seen. Therefore, the band observed at  $1016\text{ cm}^{-1}$  is most likely not an overtone, but some contamination which occurred during the preparation procedure. All the other bands that do not shift upon the  $^{16}\text{O}$ – $^{18}\text{O}$  exchange are due to vibrational modes of bpea, counterions, and solvent molecules which are part of the crystals. Changes in intensity of absorption bands, such as those at  $1121$ ,  $1109$ , and  $1097\text{ cm}^{-1}$ , are due not to isotopic exchange but to small differences in amounts of free bpea molecules, counterions, and solvent molecules between the  $^{16}\text{O}$  and  $^{18}\text{O}$  solid samples.

#### FTIR (Oxidized, $\text{Mn}^{\text{IV}}_4$ – Reduced, $\text{Mn}^{\text{III}}\text{Mn}^{\text{IV}}_3$ ) Difference Spectra of the Adamantane-like Compound in Solution.

Figures 5 and 6 show the FTIR (oxidized,  $\text{Mn}^{\text{IV}}_4$  – reduced,  $\text{Mn}^{\text{III}}\text{Mn}^{\text{IV}}_3$ ) solution difference spectra measured for the  $^{16}\text{O}$  and  $^{18}\text{O}$  compounds, respectively, using the spectroelectrochemical setup<sup>71</sup> described in the Experimental Section. Each figure contains three spectra: the difference spectrum during the reduction cycle (purple), the difference spectrum from the oxidation cycle (blue), and the Sum spectrum (black). Both figures are plotted so that features due to the  $\text{Mn}^{\text{IV}}_4$  oxidation state have a positive intensity, while the features due to the  $\text{Mn}^{\text{III}}\text{Mn}^{\text{IV}}_3$  oxidation state have a negative intensity. A distinction can be made between reversible and nonreversible signals by comparing the difference spectra collected during the reduction and oxidation cycles. Reversible signals have the same sign for the reduction and oxidation cycles, but nonreversible signals have opposite sign.

Figures 5 and 6 show nonreversible signals, indicated by ‡, at  $1100$ ,  $917$ ,  $739$ , and  $624\text{ cm}^{-1}$ , which are most likely due to decomposition of the electrolyte and solvent.<sup>71</sup> The signals indicated by an asterisk, at  $877$ ,  $844$ , and  $560\text{ cm}^{-1}$ , in Figures

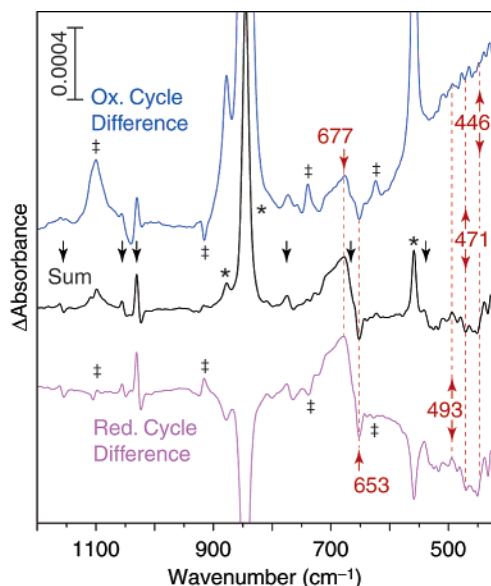


**Figure 6.** FTIR (oxidized – reduced) difference spectra of a 2.5 mM  $[\text{Mn}^{\text{IV}}_4^{18}\text{O}_6(\text{bpea})_4]^{4+}/0.1$  M  $\text{TBA}(\text{PF}_6)$  acetonitrile solution. The Sum spectrum (black) is the sum of the averaged difference spectrum from the reduction cycle (purple) and the averaged difference spectrum from the oxidation cycle (blue). The details are explained in the Experimental Section and in the caption for Figure 2. Irreversible signals due to decomposition of the electrolyte solution are indicated by ‡, and those due to changes in counterion  $\text{PF}_6^-$  concentration are indicated by \*. Reversible signals are indicated by black and red arrows, with the red arrows marking sensitivity to the  $^{16}\text{O}$ – $^{18}\text{O}$  isotopic exchange (see Figure 5). Positive reversible signals are due to the  $\text{Mn}^{\text{IV}}_4$  oxidation state, and negative signals are due to the  $\text{Mn}^{\text{III}}\text{Mn}^{\text{IV}}_3$  oxidation state.

5 and 6 are nonreversible signals due to small changes in the concentration of the electrolyte anion  $\text{PF}_6^-$ .<sup>71</sup> The Sum spectra are obtained by adding the difference spectra from the reduction cycle and a fraction of difference spectra from the oxidation cycle (see Figure 2), to minimize the nonreversible electrolyte signals over the whole spectral range (400–4000  $\text{cm}^{-1}$ , higher frequency data not shown). In the Sum spectra shown in Figures 5 and 6 the nonreversible signals are absent or reduced greatly in intensity.

Two different types of reversible signals, both sensitive to Mn oxidation state change, can be observed by comparing the Sum spectra in Figures 5 and 6. The first group of reversible signals, indicated by black arrows, corresponds to modes that have the same energy position for the  $^{16}\text{O}$  and  $^{18}\text{O}$  difference spectra. This is very clear when these spectra are directly compared in the top part of Figure 7, where the difference signals at 1162/1154, 1054/1048, 1030/1022, 773, 669/659, and at 541/528  $\text{cm}^{-1}$  do not shift on  $^{16}\text{O}$ – $^{18}\text{O}$  exchange. These bands are clearly absent in the double-difference spectrum shown in the bottom part of Figure 7, indicating that no bridging Mn–O modes are involved. These reversible signals are assigned to the changes in the vibrational modes of the terminal ligand bpea, caused by the change in Mn–bpea interaction following a change in the Mn oxidation state.

The second, more important group of reversible signals sensitive to Mn oxidation state change, indicated by red arrows, is dependent on the isotopic state of the oxygens; therefore, this indicates that bridging Mn–O modes are involved. Some of these signals are indicated by red arrows, such as the most dominant oxidized minus reduced difference signal at 709/680  $\text{cm}^{-1}$ , which shifts to 677/653  $\text{cm}^{-1}$  upon isotopic  $^{16}\text{O}$ – $^{18}\text{O}$

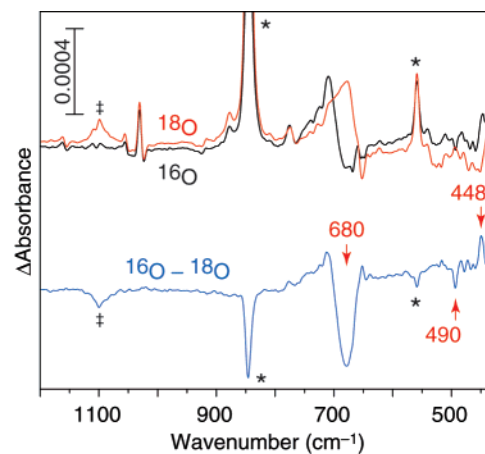


**Figure 7.** FTIR (oxidized – reduced) difference spectra of the  $^{16}\text{O}$  (black) and  $^{18}\text{O}$  (red) species, and the  $(^{16}\text{O}$ – $^{18}\text{O})$  double-difference spectrum (blue). The red arrows indicate the two regions sensitive to  $^{16}\text{O}$ – $^{18}\text{O}$  exchange. Irreversible signals due to decomposition of the electrolyte solution are indicated by ‡, and those due to changes in counterion  $\text{PF}_6^-$  concentration are indicated by \*.

exchange. This shift is even more obvious in Figure 7, where Sum spectra from both the  $^{16}\text{O}$  and  $^{18}\text{O}$  compounds are compared (top part of Figure 7), and in the double-difference spectrum shown in blue in the bottom part of Figure 7.

Other weak reversible signals, sensitive to isotopic exchange, can be observed in the 520–425  $\text{cm}^{-1}$  range in Figures 5 and 6. A positive feature is present at 510  $\text{cm}^{-1}$  in Figure 5, which could be due to the  $\text{Mn}^{\text{IV}}_4$  oxidation state, while a negative feature occurs at 493  $\text{cm}^{-1}$  in the  $\text{Mn}^{\text{III}}\text{Mn}^{\text{IV}}_3$  oxidation state. Complementary isotopically shifted peaks could be the positive feature at 493  $\text{cm}^{-1}$  and the negative band at 471  $\text{cm}^{-1}$  in Figure 6. A positive feature also appears at 446  $\text{cm}^{-1}$  in Figure 5 that is not present in Figure 6.

A direct comparison of the  $^{16}\text{O}$  and  $^{18}\text{O}$  difference spectra in Figure 7 shows that several differences occur between the two spectra in the 520–425  $\text{cm}^{-1}$  range. However, the signals are weak, and it is difficult to determine those that are reversible and sensitive to isotopic exchange in this region. To eliminate the nonisotopic sensitive signals, the double-difference spectrum of the  $^{16}\text{O}$  and  $^{18}\text{O}$  difference spectra is shown in Figure 7. This exposes only the reversible signals sensitive to  $^{16}\text{O}$ – $^{18}\text{O}$  exchange. Two strong bands appear: a negative signal at 490  $\text{cm}^{-1}$  and a positive signal at 448  $\text{cm}^{-1}$ . Additionally, some weaker double-difference signals appear between these two strong bands. This indicates that the features in the 520–425  $\text{cm}^{-1}$  range contain Mn–O modes. However, additional information from the normal-mode analysis is needed to completely understand the changes observed in the  $^{16}\text{O}$  and  $^{18}\text{O}$  difference as well as the double-difference spectra in this region.

**Normal-Mode Analysis.** Several vibrational bands in the IR spectra of the adamantane-like compound are identified as Mn–O core modes by isotopic  $^{16}\text{O}$ – $^{18}\text{O}$  exchange of the bridging oxygens. Some of these bands are sensitive to the oxidation state of the Mn atoms. Normal-mode analysis aids the assignment of the observed bands and enables us to extract specific information about the Mn–O bonds.

The adamantane-like compound contains 146 atoms and has 432 vibrational modes. Since our primary interest is in the Mn–O bridging modes of the  $\text{Mn}_4\text{O}_6$  core and only a limited number of bands can be identified, several approximations are

required to perform a normal-mode analysis of compounds **1** and **2** (a more detailed discussion is given by Visser<sup>74</sup>). The terminal bpea ligand vibrational modes are assumed to be mostly independent of the Mn–O modes and are not included in the normal-mode analysis. In addition, the Mn–N(bpea) terminal ligand interactions, expected to be below 400 cm<sup>-1</sup>, are much weaker than those of the bridging Mn–O modes and, therefore, are not included in the normal-mode analysis. Previous studies using a dinuclear Mn mono- $\mu$ -oxo compound have shown that these assumptions are reasonable and good agreement is obtained between the observed and calculated modes.<sup>62</sup>

However, if the bpea and Mn–O vibrational modes interact, a small <sup>16</sup>O→<sup>18</sup>O isotopic effect is expected for the bpea modes. In the (oxidized – reduced) difference spectra reversible signals are observed which do not shift between the <sup>16</sup>O and <sup>18</sup>O spectra and which are absent in the (<sup>16</sup>O–<sup>18</sup>O) double-difference spectrum. This indicates that these modes are not sensitive to the <sup>16</sup>O→<sup>18</sup>O exchange. All of these difference signals are at positions that correspond to the vibrational modes of the terminal ligand, bpea (Figure 3). Therefore, it is concluded that these reversible signals are caused by changes in the bpea ligand upon a change in oxidation state of Mn. This supports the assumption that the modes of the terminal ligand bpea are not influenced by the Mn–O core and can indeed be treated separately. As a result, the number of atoms considered is decreased to 10 and the number of vibrational modes to 24.

This collection consists of 12 stretching and 12 bending Mn–O modes. The bending modes are expected to be well below 400 cm<sup>-1</sup>. Including bending modes in the calculations causes only small shifts in frequencies of the stretching modes.<sup>74</sup> These shifts can be corrected by small alterations of the stretching force constants,  $\sim 0.1$  mdyn/Å. The corrections of the force constants are on the same order as the changes needed to optimize the calculated modes when a different overall symmetry is assumed. Therefore, omitting the bending force constants is reasonable, given the other approximations made for the normal-mode calculations.

Finally, some assumptions are required about the overall symmetry of the compound. If the influence of the terminal bpea ligand on **1** is ignored,  $T_d$  symmetry can be applied to the Mn<sup>IV</sup><sub>4</sub>O<sub>6</sub> core of **1**. However, if bpea is included, the highest symmetry possible is  $S_4$ . The highest possible symmetry of the Mn<sup>IV</sup><sub>3</sub>Mn<sup>III</sup>O<sub>6</sub> core of **2** is  $C_s$ , ignoring the influence of the bpea ligand. Including the bpea in the symmetry analysis reduces the symmetry to  $C_1$ , which is close to  $C_s$  symmetry. No normal-mode analysis was performed for the overall  $C_1$  symmetry because no significant additional information is obtained by including the  $C_1$  symmetry. Figure 8 shows the relation between the symmetry terms of the normal modes for the  $T_d$ ,  $S_4$ , and  $C_s$  symmetries (see Supporting Information for graphical representations of the normal modes).

**Normal-Mode Analysis of Mn<sup>IV</sup><sub>4</sub> Compound:  $T_d$  Symmetry.** When an overall  $T_d$  symmetry for **1** is assumed, the 24 vibrational modes are divided into  $2A_1$ ,  $2E$ ,  $2T_1$ , and  $4T_2$  symmetry representations. Figure 8 shows that only the triply degenerate vibrational modes with  $T_2$  symmetry are infrared active. As mentioned earlier, we will concentrate only on the Mn–O stretching modes, which have the symmetry representations  $A_1$ ,  $E$ ,  $T_1$ , and  $2T_2$ . Consequently, only two IR-active Mn–O stretching modes are anticipated. However, the IR

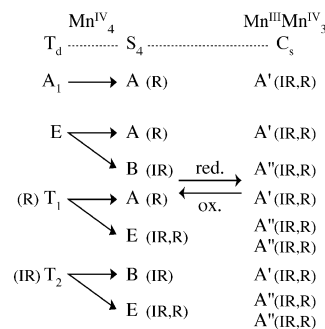


**Figure 8.** Relation among the overall symmetry representations of the Mn compound which were used for the analysis of the two oxidation states. When the influence of the terminal ligand, bpea, on the compound is ignored, the  $T_d$  and the  $C_s$  symmetries apply to the Mn<sup>IV</sup><sub>4</sub> and Mn<sup>III</sup>Mn<sup>IV</sup><sub>3</sub> compounds, respectively. When the influence of bpea on the compound is included, the  $S_4$  symmetry applies to the Mn<sup>IV</sup><sub>4</sub> species. IR and R indicate whether a symmetry term is infrared or Raman active.

**Table 1.** Comparison of the Observed and Calculated Frequencies for the [Mn<sup>IV</sup><sub>4</sub>O<sub>6</sub>(bpea)<sub>4</sub>]<sup>4+</sup> Compound<sup>a</sup>

		<sup>16</sup> O (cm <sup>-1</sup> )		<sup>18</sup> O (cm <sup>-1</sup> )		$\Delta$ (cm <sup>-1</sup> )	
symmetry		calcd		calcd		calcd	
$T_d$	$S_4$	obsd	$T_d$	$S_4$	obsd	$T_d$	$S_4$
$2T_2$	B	745	743	705	706	40	37
	E	746	748	709	711	37	37
	B	510	489	490	473	20	16
	E	508	506	492	490	16	16
$T_1$	A	707	705	674	672	33	33
	E	706	707	673	673	33	34
$E$	A		504		487		17
	B		512		497		15
$A_1$	A	503	491	485	474	18	17

<sup>a</sup> The observed IR frequencies are those of the solid compounds in KBr pellets (see also Figure 3). The optimal force constants are given for an overall  $T_d$  or  $S_4$  symmetry:  $f_{T_d}^{IV} = 3.15$  mdyn/Å,  $f_{T_d}^{III} = 0.55$  mdyn/Å, and  $f_{T_d}^{Mn} = 0.20$  mdyn/Å in the case of  $T_d$  symmetry, or  $f_{T_d}^{IV} = 3.10$  mdyn/Å,  $f_{T_d}^{III} = 0.50$  mdyn/Å, and  $f_{T_d}^{Mn} = 0.20$  mdyn/Å in the case of  $S_4$  symmetry. (For graphical representations of the normal modes, see the Supporting Information.)

absorption and difference spectra of the Mn<sup>IV</sup><sub>4</sub> compound show at least three strong absorption bands in Figure 3 at 510, 707, and 745 cm<sup>-1</sup>. Nevertheless, a normal-mode calculation was attempted to match two  $T_2$  modes to these absorption bands. Table 1 presents a normal-mode analysis which assigns the 510 and 745 cm<sup>-1</sup> vibrational modes to the  $T_2$  representation. The calculated values are similar to the observed values, including their isotopic shift. The mode at 707 cm<sup>-1</sup> is assigned to the IR-inactive  $T_1$  representation. However, this mode becomes partially active when the  $T_d$  symmetry breaks down, as shown in Figure 8.

**Normal-Mode Analysis of Mn<sup>IV</sup><sub>4</sub> Compound:  $S_4$  Symmetry.** When the symmetry of the bpea ligand is included, the  $T_2$  degenerate levels of the  $T_d$  symmetry split into the two IR-active  $E$  and  $B$  representations (Figure 8). Additionally, other vibrational modes become IR active in the  $S_4$  symmetry. One absorption is derived from the  $T_1$  symmetry representation, which splits into an IR-active doubly degenerate transition (symmetry representation  $E$ ) and a Raman-active transition (symmetry representation  $A$ ). The other new IR absorption comes from the degenerate  $E$  symmetry representation and separates into an IR- (symmetry representation  $B$ ) and a Raman-active (symmetry representation  $A$ ) vibration.

Table 1 presents the results of the normal-mode analysis, assuming  $S_4$  symmetry. The vibrational modes are organized as for  $T_d$  symmetry. The calculated values are similar to the observed values, including their isotopic shift. The  $745\text{ cm}^{-1}$  feature is calculated to be an absorption band consisting of three vibrational modes: one at  $743$  and two at  $748\text{ cm}^{-1}$ . This splitting in the  $T_2$  representation is supported by the broad bandwidth of  $\sim 20\text{ cm}^{-1}$  observed for this mode. A similar situation occurs for the  $510\text{ cm}^{-1}$  mode, where the  $T_2$  mode splits into one  $489$  and two  $506\text{ cm}^{-1}$  modes. Additionally, a new active mode in  $S_4$  symmetry occurs at  $512\text{ cm}^{-1}$ , which is derived from the  $E$  representation in  $T_d$  symmetry. This new band also contributes to the broad bandwidth of  $\sim 20\text{ cm}^{-1}$  observed for the  $510\text{ cm}^{-1}$  mode. Therefore, the bandwidths of both the  $510$  and  $745\text{ cm}^{-1}$  modes are indications that a symmetry of  $S_4$  or lower is required to explain the spectra of the  $\text{Mn}^{\text{IV}}_4$  adamantane-like compound.

Table 1 indicates that the  $707\text{ cm}^{-1}$  band is derived from the  $T_1$  symmetry representation, as suggested earlier. When the overall  $S_4$  symmetry is assumed, this band splits into an IR- and Raman-active doubly degenerate mode at  $707\text{ cm}^{-1}$  and a Raman-active mode at  $705\text{ cm}^{-1}$ . This band has a bandwidth of about  $\sim 14\text{ cm}^{-1}$ , which suggests that the doubly degenerate mode has split, indicating the distorted  $S_4$  symmetry of the adamantane-like compound.

**Normal-Mode Analysis of  $\text{Mn}^{\text{III}}\text{Mn}^{\text{IV}}_3$  Compound:  $C_s$  Symmetry.** The one-electron-reduced compound **2** approaches an overall  $C_s$  symmetry when the symmetry of the bpea ligand is neglected. Figure 8 shows that all of the degeneracies are split upon reduction of **1**, and all vibrational modes become IR and Raman active. Consequently, not only are shifts in peaks anticipated due to reduction of the compound, but also broadening of the previously degenerate modes, and new modes in the IR spectra, are expected.

The broad reversible difference signal at  $\sim 710\text{ cm}^{-1}$  resembles the signature of the ( $^{16}\text{O}$ – $^{18}\text{O}$ ) difference spectrum of the solid  $\text{Mn}^{\text{IV}}_4$  compound (Figure 4). However, unlike isotopic exchange, redox chemistry causes significant changes in bond lengths, bond angles, bond strengths, and, consequently, the overall symmetry of the compound. This results in different frequency shifts for each vibrational mode, including possible shifts to higher energy. Owing to the change in overall symmetry, certain modes will become IR active or inactive, and the isotopic shifts will also alter. Therefore, simulating the difference signal in the  $750$ – $650$  and  $520$ – $460\text{ cm}^{-1}$  ranges is not straightforward.

To reduce the complexity of the normal-mode calculations of **2**, some additional assumptions about the force constants are necessary. The stretching force constants of all  $\text{Mn}^{\text{IV}}\text{--O}$  bonds are kept at the values calculated from the solid-state spectrum of **1**,  $f_{\text{r}}^{\text{IV}} = 3.10\text{ mdy}\ddot{\text{A}}$ , and a  $\text{Mn}^{\text{III}}\text{--O}$  stretching force constant,  $f_{\text{r}}^{\text{III}}$ , is included. Introducing a second  $\text{Mn}^{\text{III}}\text{--O}$  force constant to account for Jahn–Teller distortion does not improve the fitting significantly. However, the Jahn–Teller distortion does have a significant effect on the kinetic energy matrix, which contains geometry and structural information. Hence, this structural information is included in the kinetic energy matrix for compound **2**. Two types of stretching coupling constants are used: with either oxygen,  $f_{\text{rOr}}$ , or manganese,  $f_{\text{rMnr}}$ , at the apex.

**Table 2.** Comparison of the Observed and Calculated Frequencies for the  $[\text{Mn}^{\text{III}}\text{Mn}^{\text{IV}}_3\text{O}_6(\text{bpea})_4]^{3+}$  Compound<sup>a</sup>

$C_s$	$^{16}\text{O}$ ( $\text{cm}^{-1}$ )		$^{18}\text{O}$ ( $\text{cm}^{-1}$ )		$\Delta$ ( $\text{cm}^{-1}$ )	
	obsd	calcd	obsd	calcd	obsd	calcd
$2A'$	$\sim 745$	747, 709	$\sim 705$	710, 674	$\sim 40$	37, 35
$A''$		747		710		37
$2A'$	493	492, 478	471	476, 463	22	16, 15
$A''$		464		449		15
$A'$	680	685	653	653	27	32
$2A''$		726, 689		692, 656		34, 33
$A'$		505		488		17
$A''$		500		485		15
$A'$		466		450		16

<sup>a</sup> The observed IR frequencies of the Mn–O modes are those of the electrochemical solution. Overall  $C_s$  symmetry is assumed. Bending force constants are set at zero, and stretching force constants are  $f_{\text{r}}^{\text{IV}} = 3.10\text{ mdy}\ddot{\text{A}}$ ,  $f_{\text{r}}^{\text{III}} = 2.45\text{ mdy}\ddot{\text{A}}$ ,  $f_{\text{rOr}} = 0.40$ , and  $f_{\text{rMnr}} = 0.15\text{ mdy}\ddot{\text{A}}$ . The normal modes are organized as for  $T_d$  in Table 1. (For graphical representations of the normal modes, see the Supporting Information.)

Using overall  $C_s$  symmetry and these force constant variables, the normal modes of **2** were calculated from the difference signals of the ( $\text{Mn}^{\text{IV}}_4\text{--Mn}^{\text{III}}\text{Mn}^{\text{IV}}_3$ ) difference spectra and the ( $^{16}\text{O}$ – $^{18}\text{O}$ ) double-difference spectrum (Figure 7). Four different objectives were sought with the normal-mode calculation. The first objective was to try to simulate the difference signals in the  $620$ – $720\text{ cm}^{-1}$  range for both the  $^{16}\text{O}$  and  $^{18}\text{O}$  spectra. The second objective was to match the ( $^{16}\text{O}$ – $^{18}\text{O}$ ) double-difference signal in this range. The third objective was to simulate the difference signals in the  $420$ – $520\text{ cm}^{-1}$  range for both the  $^{16}\text{O}$  and  $^{18}\text{O}$  spectra. The final objective was to obtain a simulation that matches the ( $^{16}\text{O}$ – $^{18}\text{O}$ ) double-difference signal in this range, especially the positive signals around  $510$  and  $448\text{ cm}^{-1}$  and the negative band at  $490\text{ cm}^{-1}$ .

Table 2 presents the calculated frequencies which gave a reasonable simulation of the difference and double-difference signals, as shown in Figure 9 (for graphical representations of the normal modes, see the Supporting Information). Normal-mode calculations give only the absorption frequencies of the normal modes; they do not give any information about the width or intensity of these transitions. Therefore, the intensities and bandwidths are based on the information that was obtained from the solid-state spectra. Figure 9 shows that the simulated spectra match the measured spectra reasonably well in the  $620$ – $720\text{ cm}^{-1}$  range. There are small differences between frequencies and bandwidths, but the simulated spectra contain all of the observed features. The  $^{18}\text{O}$  difference spectrum has the poorest match, which is due to the fact that the isotopic exchange is only 90% complete. Therefore, the  $^{18}\text{O}$  difference spectrum also contains signals of adamantane-like compounds with various  $^{16}\text{O}/^{18}\text{O}$  ratios, causing the observed signal to be broader than the calculated one.

It was more difficult to match the simulated signals with the observed signals in the  $425$ – $520\text{ cm}^{-1}$  range. All of the vibrational modes undergo major changes upon reduction of **1**. Therefore, it is difficult to match all of the calculated changes with the observed shifts in this range. Nevertheless, the simulations match the observed spectra reasonably well, especially the double-difference spectrum (Figure 9). Only slight shifts in some of the normal modes are needed to improve the match between simulated and observed signals. This could be achieved by including more stretching force constants, such as



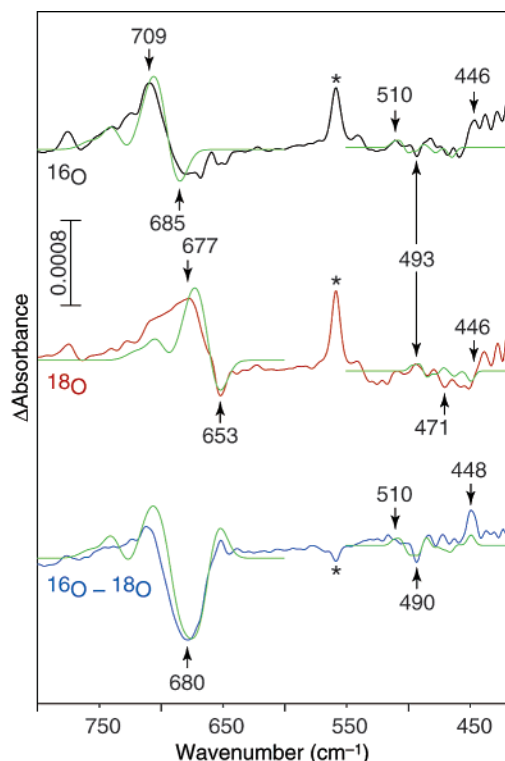


**Figure 9.** Comparison of the observed  $^{16}\text{O}$  (black) and  $^{18}\text{O}$  (red) (oxidized – reduced) difference spectra and the  $(^{16}\text{O}-^{18}\text{O})$  double-difference spectrum (blue) with the simulated spectra (green). The simulated spectra are obtained using the calculated frequencies of  $S_4$  symmetry for the  $\text{Mn}^{\text{IV}}_4$  species, Table 1, and  $C_s$  symmetry for the  $\text{Mn}^{\text{III}}\text{Mn}^{\text{IV}}_3$  species, Table 2. The arrows indicate the frequencies that were optimized. Irreversible signals due to the counterion  $\text{PF}_6^-$  are indicated by \*.

a Jahn–Teller and a non-Jahn–Teller force constant for the  $\text{Mn}^{\text{III}}\text{–O}$  bond, or coupling force constants dependent on the oxidation state of the Mn atoms. However, including more variables will not give more significant information about the compound; therefore, this expansion of variables is not presented.

**Relevance to the Mn Cluster in the Oxygen-Evolving Complex of Photosystem II.** In summary, a good match is obtained (Tables 1 and 2) between the calculated vibrational frequencies, using reasonable assumptions about symmetry and force constants, and the observed vibrational modes, indicating that this approach is valid. Sheats et al.<sup>62</sup> used a similar approach to explain their results for a mono- $\mu$ -oxo-bridged binuclear compound. One of the assumptions also made by Sheats et al.<sup>62</sup> is that the Mn–N interaction is much weaker than the  $\mu$ -oxo bridge Mn–O interaction and hence can be excluded from the normal-mode analysis. As mentioned in the Introduction, most of the ligands to the Mn cluster are carboxylate groups. Some of these carboxylate groups may be bridging ligands between Mn atoms in the OEC, which will influence the Mn–O core modes. Therefore, these interactions may need to be included in the normal-mode analysis of the OEC.

Another influence on the bridging Mn–O interaction is the number of bridging oxygens to the Mn atom. As expected, the force constant of a  $\text{Mn}^{\text{III}}\text{–O}$  bond,  $f_{\text{r}}^{\text{III}} = 2.45 \text{ mdyn}/\text{\AA}$ , is weaker than that of the  $\text{Mn}^{\text{IV}}\text{–O}$  bond,  $f_{\text{r}}^{\text{IV}} = 3.10 \text{ mdyn}/\text{\AA}$ . However, both of these values are smaller than the value found for the  $\text{Mn}^{\text{III}}\text{–O}$  bond,  $f_{\text{r}}^{\text{III}} = 3.34 \text{ mdyn}/\text{\AA}$ , of the mono- $\mu$ -oxo compound  $[\text{Mn}^{\text{III}}_2\text{O}(\text{O}_2\text{CCH}_3)_2(\text{HB}(\text{pz})_3)_2]$  ( $\text{HB}(\text{pz})_3^- = \text{hydro-$

tris(1-pyrazolyl)borate) studied by Sheats et al.<sup>62</sup> This is an indication that the strength of the Mn–X bond depends not only on the oxidation state of Mn and the electronegativity of X, but also on the character of the other bridging ligands. The manganese atoms in the adamantane-like compound have three  $\mu$ -oxo bridge oxygens. Most likely, the number of  $\mu$ -oxo bridges influences the strength of the Mn–O bonds. Therefore, it is imperative that more manganese compounds are studied to provide further insight into the behavior of these Mn–O vibrational modes and to provide more accurate models of the OEC.

The IR spectra of the oxidized compound **1** both in the solid state and in solution show three distinct bands at about 510, 707, and  $745 \text{ cm}^{-1}$ , which are assigned to the asymmetric Mn–O–Mn stretching modes. The Mn–O–Mn mode at  $707 \text{ cm}^{-1}$  shifts by  $33 \text{ cm}^{-1}$  on isotopic substitution ( $^{16}\text{O}$  with  $^{18}\text{O}$ ) of the bridging mono  $\mu$ -oxo group. The vibrational bands at 510 and  $745 \text{ cm}^{-1}$  are downshifted by 20 and  $40 \text{ cm}^{-1}$ , respectively, on  $^{18}\text{O}$  substitution. These isotopic shifts are well calculated by the normal-mode analysis. The magnitude of this shift of the Mn–O–Mn bridging frequency is typical of the downshift observed in di- $\mu$ -oxo-bridged binuclear Mn compounds where both of the bridges are substituted by  $^{18}\text{O}$ .<sup>49,56</sup> These shifts were confirmed by normal-mode analysis (data not shown). In the only other study with a binuclear mono- $\mu$ -oxo-bridged Mn compound where  $^{16}\text{O}$  was replaced by  $^{18}\text{O}$ , the downshift was from  $717$  to  $680 \text{ cm}^{-1}$ , a downshift of  $37 \text{ cm}^{-1}$  that compares well with the results of our study.<sup>62</sup>

A seminal FTIR difference study of the Mn cluster in the oxygen-evolving complex by Babcock and co-workers has identified an IR band at  $606 \text{ cm}^{-1}$  with the Mn–O–Mn stretching mode.<sup>52</sup> The band at  $606 \text{ cm}^{-1}$  shifts downward by only about  $10 \text{ cm}^{-1}$  on isotopic substitution, in contrast to the  $\sim 30 \text{ cm}^{-1}$  shift seen in the di- $\mu$ -oxo compounds in other studies (ref 49 and references therein) and in the mono- $\mu$ -oxo-bridged complex shown in this study. The small shift was attributed to partial substitution of only one of the di- $\mu$ -oxo bridges of a  $\text{Mn}_2\text{O}_2$  unit; an explanation based on the observation of a  $9 \text{ cm}^{-1}$  shift in a di- $\mu$ -oxo-bridged Mn compound with about 53% isotopic replacement.<sup>23</sup> However, other explanations are possible, such as the presence of a hydroxo-bridged group, or a hydrogen-bonding network that leads to the smaller shift on  $^{18}\text{O}$  substitution in the OEC.

On reduction of a  $\text{Mn}^{\text{IV}}$  to  $\text{Mn}^{\text{III}}$  in the electrochemical cycle of the adamantane-like compound, we observe a shift in the most intense band from  $709$  to  $680 \text{ cm}^{-1}$ , a shift of  $29 \text{ cm}^{-1}$ , and in the band at  $510$  to  $493 \text{ cm}^{-1}$ , a shift of  $17 \text{ cm}^{-1}$ . There is no shift in the third band observed at  $745 \text{ cm}^{-1}$  on reduction. All three bands are also sensitive to isotopic substitution; shifting from  $680$  to  $653$ ,  $493$  to  $471$ , and  $745$  to  $705 \text{ cm}^{-1}$  on reduction in the  $^{18}\text{O}$  compound. The shifts of 17 and  $29 \text{ cm}^{-1}$  observed on reduction in this study are in contrast to the findings in the two other studies that have probed the effect of oxidation or reduction on the Mn–O–Mn bridging vibrational bands in di- $\mu$ -oxo-bridged binuclear Mn complexes.<sup>23,56</sup> Dave and Czer-nuszewicz<sup>56</sup> report a  $1 \text{ cm}^{-1}$  downward shift on oxidation ( $\text{Mn}_2^{\text{III,IV}}$  to  $\text{Mn}_2^{\text{IV,IV}}$ ), while the study by Cooper and Calvin<sup>23</sup> reports an upward shift of about  $6 \text{ cm}^{-1}$  on oxidation. We are unaware of any other IR study using a mono- $\mu$ -oxo-bridged binuclear Mn complex with Mn oxidation states of 3+ or 4+.

Vincent and co-workers<sup>76</sup> reported that there are major changes in the vibrational frequencies of carboxylate groups ( $\sim 1400$ – $1700\text{ cm}^{-1}$ , note that these are not Mn–O bands) bridged between Mn atoms on change in oxidation state from Mn<sup>III</sup> to Mn<sup>IV</sup>. The shifts reported were as large as  $100\text{ cm}^{-1}$ . The shifts we observe are in accord with what one expects from a change in the oxidation state of the metal ion, that would be caused by a change in the force constant of the Mn–O bond involved due to a change in the Mn oxidation state change. It is very surprising, however, that we observe such a major shift on the change in the oxidation state of only one Mn atom out of four. These results clearly point to what one can expect from the OEC and also the difficulties involved in assigning the vibrational modes involved, as explained below.

In contrast, for the oxygen-evolving complex of PS II, the IR band, assigned as the Mn–O–Mn normal mode, is identified as shifting from  $625$  to  $606\text{ cm}^{-1}$  during the  $S_1$  to  $S_2$  transition,<sup>52</sup> a downward shift for a transition that is supposed to correspond to a Mn<sup>III</sup> to Mn<sup>IV</sup> oxidation.<sup>5</sup> As detailed above, with the compound that we investigated there was a major change in symmetry that would theoretically make all 12 bridging Mn–O–Mn modes IR active. However, we observed only three of these bands, and it is also possible that the bands observed in the oxidized compound are not the same modes observed in the reduced species (see the Supporting Information). The change in symmetry makes it possible that one can observe other modes. Hence, the tacit assumption that the band shifts from  $625$  to  $606\text{ cm}^{-1}$  during the  $S_1$  to  $S_2$  transition may be an oversimplification. Because of changes in symmetry upon oxidation, as seen in the adamantane-like compound, it is possible that the two bands are not the same vibrational modes and are from entirely different symmetry representations (this can be seen also in the Supporting Information). The data from the present study show that it is too simplistic to look for a one-to-one correspondence in bands on oxidation or reduction when this entails a change in symmetry of the molecule.

The disparities between the OEC and the trends seen in the adamantane-like compound could also be due to a difference in Mn–O core structure; from EXAFS it is known that the adamantane-like compound spectra do not match the PS II data.<sup>3–5,77,78</sup> Additionally, half of the ligands to the Mn atoms in the adamantane-like compound are N ligands and half are O ligands, while the majority of the Mn ligands in the OEC are O ligands.<sup>10,15,39</sup> The character of the ligands to the Mn atoms

influences the Mn–O bond strengths and consequently the vibrational modes. Therefore, one could expect to observe differences in IR spectra between the adamantane-like compound and the OEC, even if the Mn–O cores are structurally the same.

From the normal-mode analysis it is known that the adamantane-like compound has 24 vibrational modes. The overall symmetry determines whether all of these vibrational modes are IR active. However, even when all modes are dipole-allowed, their intensities may be weak. In the case of compounds **1** and **2**, only one strong, well-resolved absorption band is observed at  $707$  or  $680\text{ cm}^{-1}$ , and a broad absorption band at  $745\text{ cm}^{-1}$ . Various weaker absorption bands occur in the  $520$ – $425\text{ cm}^{-1}$  range, even though some of these vibrations are dipole-allowed in the highest symmetry. This might explain why so far only one IR band has been observed for the OEC. It is possible that the intensities of the other modes are weak and cannot be observed with the current sensitivity. Alternatively, not all modes may be IR active, depending on the overall symmetry of the OEC. It is important to observe the weaker vibrational modes of the OEC during the catalytic cycle to have an informative interpretation of the IR data. These bands might be easier to observe using Raman spectroscopy, as some might be formally allowed transitions. For example, in the case of compound **1**, the  $A_1$  mode in  $T_d$  symmetry is not observed because it is IR inactive, but this mode should be observed in the Raman spectrum.

Development of a novel spectroelectrochemical technique enabled us to study IR (oxidized – reduced) difference solution spectra, with good signal-to-noise ratio and at low concentrations of the adamantane-shaped  $\{\text{Mn}_4\text{O}_6\}$  core. This method allowed us to study homologous compounds in different oxidation states, which are relevant to the catalytic cycle of the oxygen-evolving complex in photosystem II. These IR spectra and their analysis provide additional means for the interpretation of the vibrational modes of other model compounds, as well as for the OEC.

**Acknowledgment.** The authors thank Dr. Heinz Frei (Lawrence Berkeley National Laboratory) for the use of the Bruker IFS88 FTIR spectrometer. This research was supported by the Director, Office of Science, Office of Basic Energy Sciences, Division of Energy Biosciences, U.S. Department of Energy, under Contract DE-AC03-76SF00098 and by the National Institutes of Health Grant GM 55302.

**Supporting Information Available:** Graphical representation of the vibrational normal modes of the adamantane-like compound (PDF). This material is available free of charge via the Internet at <http://pubs.acs.org>.

JA020409J

- (76) Smith, J. C.; Gonzalez-Vergara, E.; Vincent, J. B. *Inorg. Chim. Acta* **1997**, *255*, 99–103.  
(77) Liang, W.; Roelofs, T. A.; Cinco, R. M.; Rompel, A.; Latimer, M. J.; Yu, W. O.; Sauer, K.; Klein, M. P.; Yachandra, V. K. *J. Am. Chem. Soc.* **2000**, *122*, 3399–3412.  
(78) DeRose, V. J.; Mukerji, I.; Latimer, M. J.; Yachandra, V. K.; Sauer, K.; Klein, M. P. *J. Am. Chem. Soc.* **1994**, *116*, 5239–5249.